Angewandte Chemie International Edition

Angewandte International Edition Chemie

How to cite: *Angew. Chem. Int. Ed.* **2026**, 65, e4716315
doi.org/10.1002/anie.4716315

RESEARCH ARTICLE Hot Paper

Incorporation of Engineered Cu^0/Cu^+ Interfaces in Metal-Organic Frameworks for Boosting CO_2 Hydrogenation to Methanol

Xiao-Mei Lei[1] | Jiajia Huang[1,2] | Li-Li Ling[1,3] | Jiayi Xu[1] | Ming-Liang Gao[1] | Jingyao Liu[4] | Hai-Long Jiang[1,5]

[1]Hefei National Research Center for Physical Sciences At the Microscale, Department of Chemistry, University of Science and Technology of China, Hefei, Anhui, P. R. China | [2]Fujian Provincial Key Laboratory of Soil Environmental Health and Regulation, College of Resources and Environment, Fujian Agriculture and Forestry University, Fuzhou, P. R. China | [3]Institute of Future Technologies, Deep Space Exploration Laboratory, Hefei, Anhui, P. R. China | [4]Institute of Theoretical Chemistry, College of Chemistry, Jilin University, Changchun, Jilin, P. R. China | [5]Department of Radiation Oncology, Division of Life Sciences and Medicine, The First Affiliated Hospital of USTC, University of Science and Technology of China, Hefei, Anhui, P.R. China

Correspondence: Hai-Long Jiang (jianglab@ustc.edu.cn)

Received: 19 January 2026 | **Revised:** 27 May 2026 | **Accepted:** 9 June 2026

Keywords: CO_2 hydrogenation | copper nanoparticle | heterogeneous catalysis | metal-organic framework | microenvironment modulation

ABSTRACT

The Cu-based materials are an important category of catalysts for CO_2 hydrogenation to methanol, in which Cu^0 and Cu^+ species have been widely acknowledged to play key roles in the reaction. Herein, a series of metal-organic frameworks (MOFs), namely UiO-66(n) with exposed —COOH groups, are fabricated by employing both terephthalic acid and 1,2,4-benzenetricarboxylic acid linkers. Following by introducing Cu nanoparticles, Cu@UiO-66(n) are synthesized. By regulating the amount of exposed —COOH groups on the MOF pore wall, the interaction between Cu and the MOF support is regulated. This —COOH microenvironment regulates the overall Cu^0/Cu^+ ratio in the supported Cu species, thereby tuning the Cu^0/Cu^+ interfacial descriptor, which is closely associated with the CO_2 hydrogenation performance. The Cu@UiO-66(25) featuring the longest Cu^0/Cu^+ interface achieves a methanol space-time yield of 694 g kg_{cat}^{-1} h^{-1} and methanol selectivity of 92.8% at 250 °C and 4 MPa, far surpassing other counterparts. This work provides a deep understanding of the synergistic effect between Cu^0 and Cu^+ species in catalytic CO_2 hydrogenation.

1 | Introduction

The sustained increase in CO_2 emissions has led to severe environmental challenges, creating a compelling necessity to convert CO_2 into high-value fuels and chemicals [1–3]. Methanol, serving as a fundamental chemical feedstock and an important energy carrier, exhibits extensive applications across various fields, thereby possessing substantial economic value [3–6]. The catalytic conversion of green hydrogen and CO_2 into methanol can effectively reduce CO_2 emissions, offering a promising approach for realizing the resource utilization of CO_2 and contributing to carbon neutrality [7–9]. Given the high stability of CO_2 molecules, methanol synthesis by CO_2 hydrogenation typically requires reaction conditions of high temperature (450–600 K) and high pressure (20–100 atm) [10–15].

Copper (Cu)-based catalysts represent a significant class of catalytic materials for the hydrogenation of CO_2 to methanol due to their cost-effectiveness and excellent reaction performance under moderate reaction temperatures [16, 17]. Cu nanoparticles (NPs) serve as the metallic active centers, whose surface and electronic properties are intricately correlated with the resulting catalytic

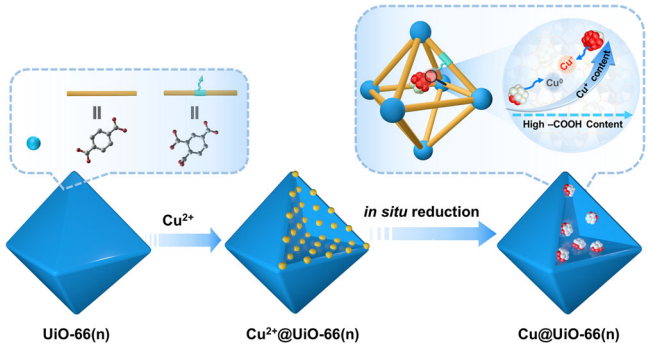

SCHEME 1 | Illustration showing the synthetic strategy for Cu@UiO-66(n) with different content of exposed —COOH groups.

activity [18]. However, Cu exhibits versatile redox properties, leading to the coexistence of multiple Cu species (Cu^0, $Cu^{\delta+}$/Cu^+) under real reaction conditions [19–21]. Metallic Cu^0 in Cu NPs is widely regarded as the key site for H_2 dissociation, while electron-deficient Cu^+ species at the metal-support interface can enhance the adsorption of key oxygenate intermediates such as *CO and HCOO* [22–25]. Notably, efficient further hydrogenation of the HCOO* intermediate is critical, as insufficient conversion leads to its accumulation on the catalyst surface [24]. Importantly, Cu^+ species are proven to effectively stabilize the HCOO* intermediate, thereby facilitating its subsequent conversion to methanol, which offers a direction for rational design of high-performance Cu-based catalysts [26, 27].

However, supported Cu-based CO_2 hydrogenation catalysts constitute a highly complex and dynamic system, whose activity is influenced by a multitude of intricately intertwined factors [12, 28–31], which makes it challenging to decouple the real roles of Cu^+ species. Furthermore, achieving continuous and precise control over the Cu^+ content in conventional Cu-based catalysts also remains a significant challenge. It is thus imperative to construct a well-defined model catalytic system that allows for precise and systematic control of Cu^+ content while fixing other parameters, which is crucial to understand how Cu^0 and Cu^+ sites interplay in the CO_2 hydrogenation.

Metal-organic frameworks (MOFs) are porous crystalline materials with high surface areas and tailorable structures [32–35]. Their pore structures provide confinement effects that stabilize metal NPs and prevent their agglomeration [36–39]. Furthermore, rational functionalization of organic linkers offers a versatile strategy for modulating the electronic states of incorporated metal centers [40, 41]. The precise control at the atomic level makes MOFs, particularly Zr-based MOFs with excellent structural stability and tailorability [39, 40, 42], an ideal platform to investigate the roles of Cu^+ and Cu^0 sites in CO_2 hydrogenation.

Herein, UiO-66(n) with varying content of exposed —COOH groups are fabricated, followed by incorporating Cu NPs to afford Cu@UiO-66(n) (n = 0, 5, 10, 25, 40, 75, representing the molar ratio of 1,2,4-benzenetricarboxylic acid among all linkers in UiO-66(n)) for CO_2 hydrogenation (Scheme 1). The dangling —COOH groups on the MOF pore wall interact with encapsulated Cu NPs, generating Cu^+ species on the interface. The amount of exposed —COOH groups creates a particular microenvironment that influences the Cu^0/Cu^+ ratio and regulates the Cu^0/Cu^+ interfacial perimeter, which is identified to play a critical role in CO_2 hydrogenation. Specifically, the HCOO* species adsorbed on Cu^+ sites is hydrogenated by H_2 activated at neighboring Cu^0 sites. As a result, Cu@UiO-66(n) exhibits a volcano-shaped performance trend with increasing —COOH content, where Cu@UiO-66(25) with the longest Cu^0/Cu^+ interface demonstrates superior performance, achieving a methanol selectivity of 92.8% and a space-time yield of 694 g kg_{cat}^{-1} h^{-1} at 250 °C and 4 MPa.

2 | Results and Discussion

A series of UiO-66(n) with varying amounts of exposed —COOH groups were synthesized based on mixed linkers of terephthalic acid and 1,2,4-benzenetricarboxylic acid via a solvothermal method. Subsequently, the pristine UiO-66(n) was dispersed in an acetonitrile solution of Cu^{2+}, and stirred at 80 °C to give Cu^{2+}@UiO-66(n). Then, the obtained samples were in situ reduced at 275 °C and 4 MPa under a CO_2/H_2 (1/3) atmosphere to afford Cu@UiO-66(n) (refer to supporting information, Experimental Section). Scanning electron microscopy (SEM) observation shows that all these MOFs possess an octahedral morphology (Figure S1). Powder x-ray diffraction (PXRD) patterns indicate that all MOFs exhibit similar crystallinity and structures to the pristine UiO-66 (Figure S2). ^{1}H NMR analysis of the digested UiO-66(n) samples confirms that the actual 1,2,4-benzenetricarboxylic acid content in the skeleton agrees well with the feed ratio (Figure S3). Upon the incorporation of Cu species, the MOF crystallinity remains well, and no discernible diffraction peak associated with Cu is observed (Figure S4). N_2 sorption results indicate that an increased amount of exposed —COOH groups in the MOF leads to a corresponding decrease in its specific surface area (Figure S5). This is reasonable as the MOF pore might be partially occupied by the dangling and additional —COOH groups. The inherent microporous architectures of UiO-66(n) are retained after Cu^{2+} decoration, albeit with partially decreased surface areas (Figure S6). Thermogravimetric analysis (TGA) reveals that UiO-66(n) exhibit similar thermal stability (Figure S7), and the corresponding MOF samples maintain good thermal stability after Cu incorporation (Figure S8).

Diffuse reflectance infrared Fourier transform spectroscopy (DRIFTS) is adopted to elucidate the interaction sites of Cu species within the MOF. In comparison to UiO-66(0)/UiO-66(25), the infrared peak intensity at ~3670 cm^{-1}, attributed to —OH/OH_2 groups, exhibits a significant decrease upon introducing of Cu^{2+} (Figures S9 and S10). This signifies the interaction between Cu^{2+} and the —OH/OH_2 groups, suggesting that Cu^{2+} is anchored to the Zr—OH groups of unsaturated Zr-oxo clusters [40, 43]. After reduction of Cu^{2+} to Cu NPs, the peak intensity of —OH/OH_2 groups is recovered, supporting that Cu^{2+} detaches from the —OH groups. Transmission electron microscope (TEM) images demonstrate no large or obviously aggregated Cu NPs for Cu^{2+}-incorporated UiO-66(25), both before and after the in situ reduction (Figure 1a,b). High-angle annular dark field scanning transmission electron microscopy (HAADF-STEM) combined with energy-dispersive x-ray spectroscopy (EDS) elemental mapping further verifies the uniform dispersion of Cu species throughout the MOF particle, and no distinguishable Cu NPs can be directly identified (Figure 1c–f). To further examine the

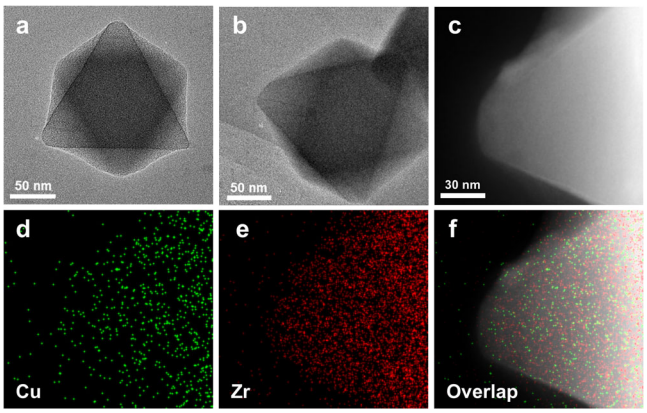

FIGURE 1 | (a) TEM image of Cu^{2+}@UiO-66(25) before in situ reduction. (b) TEM image, (c) HAADF-STEM image, and (d–f) the corresponding EDS mapping images of Cu@UiO-66(25).

confined Cu nanoparticles, the UiO-66 framework in Cu@UiO-66(25) was digested. TEM image after framework digestion shows Cu nanoparticles with sizes of approximately 2–3 nm (Figure S11). The Cu loading is verified to be similar across all samples based on the inductively coupled plasma atomic emission spectroscopy (ICP-AES) results (Table S1). The dispersion of Cu has been further examined to be 48.1% for Cu@UiO-66(25), by using N_2O oxidation followed by CO temperature-programmed desorption (TPD), corresponding to an estimated average Cu nanoparticle size of 2.1 nm (Figure S12 and Table S2), which is consistent with the TEM results. Similar average Cu sizes of 2–3 nm are estimated across the other samples, supporting the high dispersion of Cu species and suggesting no significant differences in Cu NPs size (refer to Supporting Information-Section 7).

To understand the influence of exposed —COOH groups within MOF pores on the interaction between Cu species and the UiO-66 support, H_2 temperature-programmed reduction (H_2-TPR) was performed (Figure 2a). The H_2-TPR profiles exhibit a remarkable difference in the reduction temperature (200 °C vs. 330 °C) of Cu species in Cu^{2+}@UiO-66(0) and Cu^{2+}@UiO-66(25) before in situ reduction. This result indicates that the exposed -COOH microenvironment in UiO-66(25) strengthens the interaction of the MOF support with Cu^{2+}, thereby causing the elevation of the reduction temperature [44, 45]. X-ray photoelectron spectroscopy (XPS) analysis indicates that the Cu species in both Cu^{2+}@UiO-66(0) and Cu^{2+}@UiO-66(25) before in situ reduction are predominantly in a +2 oxidation state with Cu $2p_{3/2}$ binding energy at 933.6 eV (Figure S13). The Cu 2p spectra after in situ reduction indicate that Cu^{2+} species are reduced to Cu^0/Cu^+ (Figure 2b and Figure S14) [46]. The Cu LMM Auger electron spectroscopy (AES) spectra indicate that the presence of exposed —COOH groups within MOF pore walls lowers the Cu^0/Cu^+ ratio (Figures 2c,e and S15).

In situ DRIFTS experiments using CO as a probe (CO-DRIFTS) have been conducted to provide further insights into the surface electronic state of Cu (Figures 2d and S16). The three adsorption bands located at 2116-2112, 2107-2099, and 2095-2089 cm^{-1} are attributed to Cu^+ sites, defective Cu^0 sites, and terrace Cu^0 sites, respectively [47–50]. The deconvolution analysis enables the proportion quantification of different Cu species within the catalyst. The results reveal a negative correlation between exposed

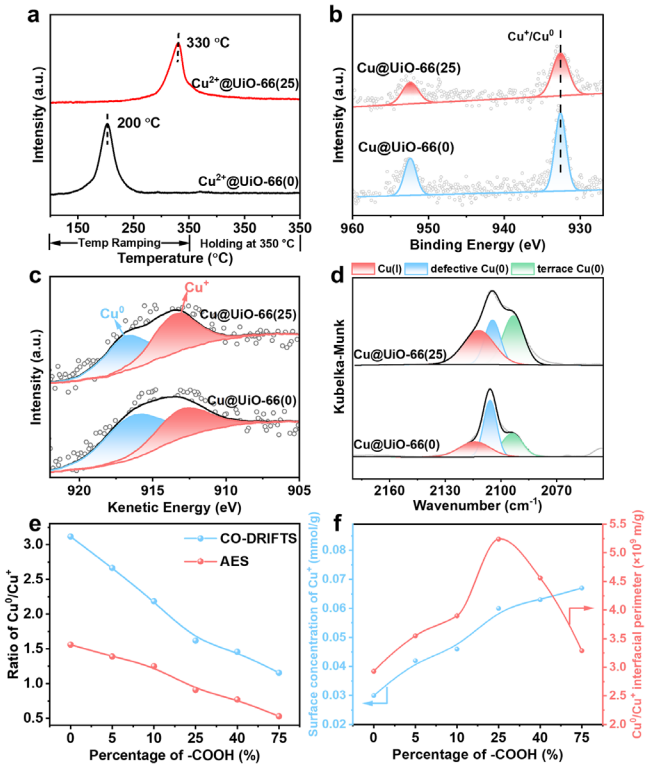

FIGURE 2 | (a) H_2-TPR profiles of Cu^{2+}@UiO-66(0) and Cu^{2+}@UiO-66(25) before in situ reduction; (b) the Cu 2p XPS spectra and (c) Cu LMM AES spectra of Cu@UiO-66(0) and Cu@UiO-66(25). (d) In situ DRIFTS spectra of CO adsorption on Cu@UiO-66(0) and Cu@UiO-66(25). (e) The evaluated ratio of Cu^0/Cu^+ on Cu@UiO-66(n) obtained from the CO-DRIFTS and AES results. (f) The surface concentration of Cu^+ and Cu^0/Cu^+ interfacial perimeter on Cu@UiO-66(n) according to N_2O oxidation followed by H_2-TPR and N_2O oxidation followed by CO-TPD results.

—COOH group content and the ratio of Cu^0/Cu^+ in Cu@UiO-66(n), which is consistent with the AES results (Figure 2e). The FT-IR results further support the interaction between exposed —COOH groups and Cu species, suggesting that the —COOH groups contribute to the regulation of Cu^+ species in Cu@UiO-66(n) (Figure S17). Furthermore, the surface concentrations of Cu^0 ($C_{Cu(0)}$) and Cu^+ ($C_{Cu(I)}$), along with the interfacial perimeter between Cu^0 and Cu^+ ($L_{Cu(0)\text{-}Cu(I)}$), have been quantified for all catalysts based on N_2O oxidation followed by H_2-TPR and N_2O oxidation followed by CO-TPD results (Figures S12 and S18; Table S2) [21, 46, 51–53]. Consistent with the CO-DRIFTS and AES results, the surface concentration of Cu^+ is successfully regulated by the —COOH microenvironment around the Cu NPs, which demonstrates a clear positive correlation with the exposed —COOH group content (Figure 2f). Interestingly, the $L_{Cu(0)\text{-}Cu(I)}$ displays a distinctive volcano-shaped trend along with increasing exposed —COOH content (Figure 2f).

Encouraged by the above results, the CO_2 hydrogenation over Cu@UiO-66(n) is evaluated under the conditions of 150–250 °C and 4 MPa ($CO_2/H_2 = 1/3$). The methanol space-time yield (STY) exhibits a consistent increase with rising reaction temperature for all investigated catalysts (Figure S19). The CO_2 conversion over Cu@UiO-66(n) at 250 °C displays a volcano-shaped trend

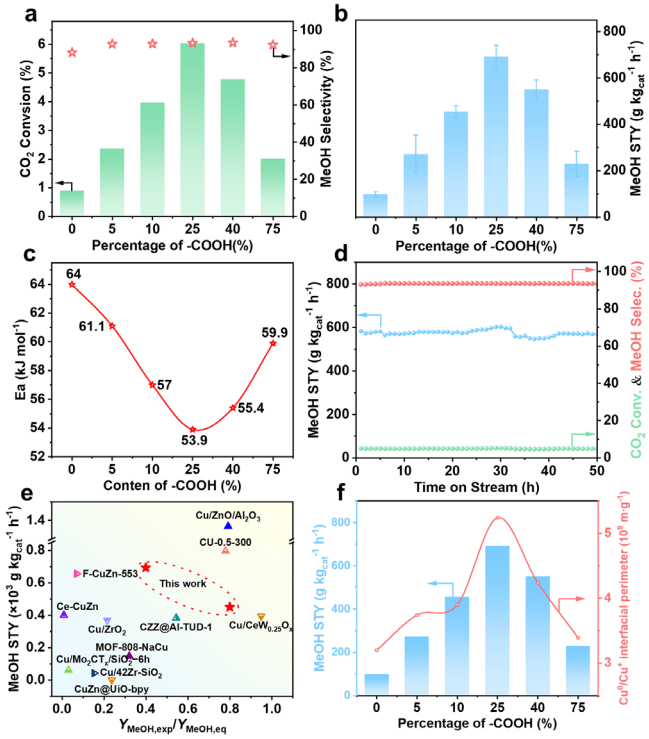

FIGURE 3 | Catalytic performance for CO_2 hydrogenation. (a) The CO_2 conversion and selectivity to methanol along with increasing percentage of exposed —COOH in Cu@UiO-66(n). (b) The methanol STY over Cu@UiO-66(n). (c) Apparent activation energies (Ea) along with increasing percentage of exposed —COOH in Cu@UiO-66(n). (d) Time-on-stream test results of Cu@UiO-66(25). (e) Comparison of the catalytic performance of the Cu@UiO-66(25) catalyst with previously reported Cu-based catalysts [14, 19, 39, 54–60]. Reaction conditions: P = 4 MPa, T = 250 °C, GHSV = 36000 mL g_{cat}^{-1} h^{-1}. (f) The methanol STY and Cu^0/Cu^+ interfacial perimeter vary with increasing percentage of exposed —COOH in Cu@UiO-66(n).

with increasing concentration of exposed —COOH groups within the MOF pores, though they all exhibit very high selectivity (88.2-93.5% at 250 °C) to methanol (Figure 3a). Amongst them, Cu@UiO-66(25) achieves the optimal performance, with methanol STY of 694 g kg_{cat}^{-1} h^{-1} and methanol selectivity of 92.8% (Figure 3a,b). Only a minimal amount of CO by-product can be detected in the gas-phase products, with no methane formation during the reaction. Moreover, upon decreasing the GHSV from 36000 to 12000 mL g_{cat}^{-1} h^{-1}, the CO_2 conversion of Cu@UiO-66(25) increases to 12.4%, with a methanol STY of 451 g kg_{cat}^{-1} h^{-1} and a methanol selectivity of 90.1% (Table S3). The apparent activation energy (Ea) of Cu@UiO-66(n) is calculated based on the activity at different temperatures and the corresponding Arrhenius plots (Figures 3c and S20), in which Cu@UiO-66(25) exhibits the lowest value of 53.9 kJ mol^{-1}. Moreover, the methanol STY and selectivity of Cu@UiO-66(25) remains well preserved over 50 h on stream under the condition of 250 °C and 4 MPa, demonstrating its remarkable stability (Figure 3d). A comparison with the reported Cu-based catalysts highlights the superior performance of Cu@UiO-66(25) in CO_2 hydrogenation, as evidenced by both the Cu-normalized productivity comparison and the equilibrium-referenced analysis (Figure 3e, Figure S21, and Table S3). Its activity reaches an impressive value of 38,556 g_{MeOH} kg_{Cu}^{-1} h^{-1} when normalized to the Cu loading.

Moreover, the MOF crystallinity is well maintained, and the Cu NPs remain well dispersed throughout the MOF particle after the reaction (Figures S22 and S23). Combined CO-DRIFTS, N_2O oxidation followed by H_2-TPR, and N_2O oxidation followed by CO-TPD results demonstrate that the ratio of Cu^0/Cu^+ and the Cu^0/Cu^+ interfacial perimeter in Cu@UiO-66(25) after reaction are comparable to those of the fresh sample (Figures S24 and S25; Table S2). These unambiguously support the structural stability of Cu@UiO-66(25) during the reaction.

Besides, UiO-66 and UiO-66(25) showcase negligible activity for CO_2 hydrogenation (Figure S26), revealing that Cu NPs serve as real active sites for this reaction. To identify the active sites in Cu@UiO-66(n), CO_2-TPD and H_2-TPD have been performed. The CO_2-TPD results demonstrate that the CO_2 desorption temperatures are similar across UiO-66(0), UiO-66(25), and all Cu@UiO-66(n) samples (Figure S27a). Quantitative analysis of the desorbed CO_2 reveals that the CO_2 adsorption capacity of these samples is comparable (Figure S27b). These results suggest that the CO_2 adsorption sites on Cu@UiO-66(n) would originate from the coordinatively unsaturated Zr-oxo clusters within the MOF [39, 42, 50]. The increased content of exposed —COOH groups and the variation in the ratio of Cu^0/Cu^+ exert negligible influence on CO_2 adsorption. In contrast, the H_2-TPD results for Cu@UiO-66(n) display significant differences, and the pristine UiO-66(0) and UiO-66(25) supports show negligible H_2 chemisorption (Figure S28). The adsorbed H_2 amount decreases with an increased concentration of exposed —COOH groups in Cu@UiO-66(n), aligning with the ratio variation of Cu^0/Cu^+ (Figure S29). Therefore, the Cu^0 species in Cu@UiO-66(n) should be the active site for H_2 adsorption and dissociation [25]. By regulating the concentration of exposed —COOH groups dangling on the MOF pore walls, the ratio of Cu^0/Cu^+ can be tuned, which in turn affects the efficiency of H_2 activation, without altering its CO_2 adsorption capacity. Given the comparable Cu loadings and similar average Cu sizes among Cu@UiO-66(n), the activity presents a positive correlation with the Cu^0/Cu^+ interfacial descriptor, suggesting that both Cu^0 and Cu^+ species jointly contribute to and play important roles in the catalysis (Figure 3f).

To gain deep insights into the reaction mechanism of CO_2 hydrogenation, the evolution of surface species on Cu@UiO-66(0) and Cu@UiO-66(25) during the reaction has been monitored using in situ DRIFTS under a CO_2/H_2 atmosphere (H_2/CO_2 = 3) at 523 K (Figures 4a, b). Upon the introduction of the feed gas to the catalyst, absorption peaks at 2742, 2842, 2857, 2877, 2968, and 2989 cm^{-1} attributed to the characteristic bands of formate species (HCOO*) can be observed [20, 42, 61]. Meanwhile, infrared bands corresponding to methoxy species (CH_3O*) at 2823, 2921, and 2938 cm^{-1} are detected. These results suggest that CO_2 is predominantly converted to methanol via the formate pathway on Cu@UiO-66(0) and Cu@UiO-66(25). Given that the binding strength of key reaction intermediates is very important in determining the methanol production rate, the electronic properties of Cu NPs might significantly affect the binding strength of the intermediates [26]. The Cu^+ species have been reported to effectively enhance the transformation of oxygen-containing

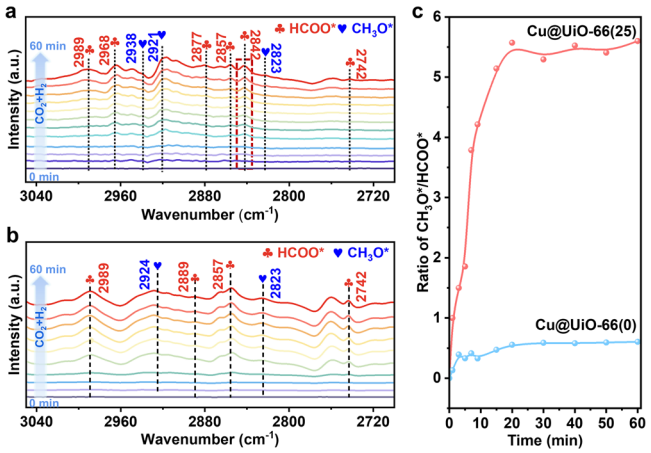

FIGURE 4 | In situ DRIFTS spectra of the CO_2 hydrogenation reaction over (a) Cu@UiO-66(25) and (b) Cu@UiO-66(0) in the range of 3050-2700 cm^{-1}. (c) The signal intensity ratio of CH_3O^* (2924/2921 cm^{-1}) to HCOO* (2857 cm^{-1}) intermediates on the surface of Cu@UiO-66(25) and Cu@UiO-66(0) as a function of reaction time.

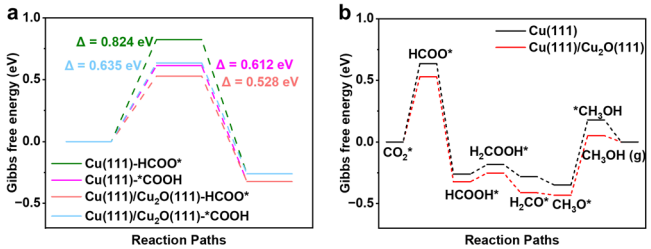

FIGURE 5 | DFT results for H*-assisted CO_2 hydrogenation to methanol on Cu(111) and Cu(111)/Cu_2O(111). (a) Calculated activation barriers for the first hydrogenation of adsorbed CO_2 by surface H* to form HCOO* and *COOH on Cu(111) and Cu(111)/Cu_2O(111). (b) Gibbs free energy profile for the subsequent formate-mediated hydrogenation pathway on Cu(111) and Cu(111)/Cu_2O(111). In these calculations, H* is treated as a pre-formed surface hydrogen species, and the H_2 dissociation step is not explicitly included.

intermediates by inducing polarization of the C═O bond [23, 25]. In the IR spectra of Cu@UiO-66(25), the characteristic band at 2842 cm^{-1}, typically ascribed to HCOO* adsorbed on Cu (HCOO*-Cu), is absent in the Cu@UiO-66(0) spectra. Previous studies have demonstrated that the reactivity of HCOO*-Cu is markedly superior to that of HCOO* bound to ZrO_2 [61, 62]. Considering the similar Cu loading in Cu@UiO-66(0) and Cu@UiO-66(25) and the higher Cu^+ content in the latter, the appearance of the HCOO*-Cu band over Cu@UiO-66(25) indicates that Cu^+ species are involved in HCOO* adsorption, which may contribute to the enhanced CO_2 hydrogenation activity of Cu@UiO-66(25).

To elucidate the dynamic behavior of intermediates on the surfaces of Cu@UiO-66(0) and Cu@UiO-66(25) during the reaction, the absorption peaks at 2924 and 2857 cm^{-1} for Cu@UiO-66(0), as well as at 2921 and 2857 cm^{-1} for Cu@UiO-66(25), are selected to monitor the evolution of CH_3O^* and HCOO* during the reaction (Figure 4c). The ratio of CH_3O^*/HCOO* signal intensity on Cu@UiO-66(25) is significantly higher than that on Cu@UiO-66, highlighting an accelerated conversion rate of HCOO* species on the surface of Cu@UiO-66(25).

In order to investigate the stabilization effect of Cu^+ species for the HCOO* intermediate, the characteristic vibrational peaks at 2855 and 2743 cm^{-1} are selected to study the behavior of HCOO* species under CO_2/H_2 and Ar atmospheres. After Ar purging for 30 min, these bands almost disappear on Cu@UiO-66(0), partially decrease on Cu@UiO-66(10), and show slight changes on Cu@UiO-66(25) (Figures S30–S32). These results indicate the pivotal role of the generated Cu^+ species density in the catalyst toward stabilizing HCOO* intermediates. Unfortunately, an increase in the ratio of Cu^+ inevitably reduces the Cu^0 content in the catalyst, thereby weakening its ability to activate H_2. As a result, the activity is not invariably improved by an increased proportion of Cu^+ species in the catalyst, and does not exhibit a strong positive correlation with either Cu^+ or Cu^0 content.

Instead, it is significantly associated with the interfacial perimeter between Cu^0 and Cu^+ species (Figure 3f). At the Cu^0/Cu^+ interface, Cu^0 species actively facilitate the adsorption and dissociation of H_2, while adjacent Cu^+ sites stabilize HCOO* intermediates. This synergistic effect accelerates the conversion of Cu^+-HCOO* intermediates into CH_3OH [24].

Furthermore, DFT calculations have been performed to gain mechanistic insight into the importance of the Cu^0/Cu^+ interfacial sites in CO_2 hydrogenation. In this work, the Cu(111) slab represents the metallic Cu^0 sites, while the Cu(111)/Cu_2O(111) heterojunction serves as an idealized local motif for the Cu^0/Cu^+ interfacial sites in Cu@UiO-66(n) (Figure S33). This model does not assume two completely separate Cu and Cu_2O phases in the catalyst. It describes the local coordination and electronic environment at the Cu^0/Cu^+ boundary and compares the intrinsic CO_2 hydrogenation energetics on Cu^0 and Cu^0/Cu^+ interfacial sites. H* was introduced as a pre-formed surface hydrogen species, which is assumed to originate from H_2 dissociation on Cu^0 sites under the reaction atmosphere. The H_2 dissociation step itself was not included in the present DFT calculations. The activation barriers for the first H*-assisted hydrogenation of adsorbed CO_2 to form HCOO* or *COOH are compared (Figure 5a). The results reveal a pronounced preference for the formate (HCOO*) pathway over the trans-*COOH route on these two structures, which is consistent with the in situ DRIFTS results (Figures 5a and S34). Moreover, Gibbs free energy calculations for the formate-mediated CO_2 hydrogenation pathway reveal that the Cu^0/Cu^+ interfacial model facilitates the formation of the HCOO* intermediate and its further conversion to methanol (Figures 5b, S35, and S36).

3 | Conclusion

In summary, a series of Cu@UiO-66(n) have been prepared through facile impregnation and subsequent in situ reduction, wherein tiny Cu NPs are distributed throughout the MOF particle. By altering the concentration of exposed —COOH groups dangling on the MOF pore walls, the interaction strength between Cu NPs and their surrounding microenvironment is controlled, which regulates the Cu^0/Cu^+ ratio and Cu^0/Cu^+ interfacial perimeter on the surface of Cu NPs. As a result, Cu@UiO-66(25) featuring the longest Cu^0/Cu^+ interface exhibits excellent cat-

alytic performance in CO_2 hydrogenation, achieving a methanol space-time yield of 694 g kg_{cat}^{-1} h^{-1} at 250 °C and >92% methanol selectivity within the temperature range of 150–250 °C, surpassing all other counterparts. At the Cu^0/Cu^+ interfacial sites, the Cu^0 adsorbs and dissociates H_2, while neighboring Cu^+ effectively stabilizes the HCOO* intermediates, promoting the conversion of Cu-HCOO* into CH_3O* and subsequently into methanol. This work unambiguously unveils the synergistic mechanism between Cu^0 and Cu^+ species in Cu-based catalysts for CO_2 hydrogenation, providing a unique perspective and design rule for the development of high-performance Cu-based catalysts toward CO_2 hydrogenation.

Author Contributions

Xiao-Mei Lei: data curation, investigation, validation, formal analysis, writing – original draft, and writing – review and editing. **Jiajia Huang**: formal analysis, investigation, and methodology. **Li-Li Ling**: formal analysis and investigation. **Jiayi Xu**: investigation and data curation. **Ming-Liang Gao**: formal analysis. **Jingyao Liu**: software, resources, and formal analysis. **Hai-Long Jiang**: conceptualization, resources, supervision, writing – review and editing, validation, formal analysis, project administration, funding acquisition, and software.

Acknowledgments

This work was supported by the Strategic Priority Research Program of the Chinese Academy of Sciences (XDB0540000), National Key Research and Development Program of China (2021YFA1500400), the National Natural Science Foundation of China (22331009, U22A20401, W2512006, 22575234 and 22301186) and the Key Project of Natural Science Foundation of Anhui Province (2508085ZD002). This work was partially carried out at the Instruments Center for Physical Science, USTC.

Conflicts of Interest

The author declares no conflicts of interest

Data Availability Statement

The data that support the findings of this study are available from the corresponding author upon reasonable request.

References

1. J. Artz, T. E. Müller, K. Thenert, et al., "Sustainable Conversion of Carbon Dioxide: An Integrated Review of Catalysis and Life Cycle Assessment," *Chemical Reviews* 118 (2018): 434–504, https://doi.org/10.1021/acs.chemrev.7b00435.

2. M. Ding, R. W. Flaig, H.-L. Jiang, and O. M. Yaghi, "Carbon Capture And Conversion Using Metal–Organic Frameworks and MOF-Based Materials," *Chemical Society Reviews* 48 (2019): 2783–2828, https://doi.org/10.1039/C8CS00829A.

3. J. Ye, N. Dimitratos, L. M. Rossi, N. Thonemann, A. M. Beale, and R. Wojcieszak, "Hydrogenation of CO_2 for Sustainable Fuel And Chemical Production," *Science* 387 (2025): eadn9388, https://doi.org/10.1126/science.adn9388.

4. G. A. Olah, "Beyond Oil and Gas: The Methanol Economy," *Angewandte Chemie International Edition* 44 (2005): 2636–2639, https://doi.org/10.1002/anie.200462121.

5. P. Tian, Y. Wei, M. Ye, and Z. Liu, "Methanol to Olefins (MTO): From Fundamentals to Commercialization," *ACS Catalysis* 5 (2015): 1922–1938, https://doi.org/10.1021/acscatal.5b00007.

6. C. Filosa, X. Gong, A. Bavykina, A. D. Chowdhury, J. M. R. Gallo, and J. Gascon, "Enabling the Methanol Economy: Opportunities and Challenges for Heterogeneous Catalysis in the Production of Liquid Fuels via Methanol," *Accounts of Chemical Research* 56 (2023): 3492–3503, https://doi.org/10.1021/acs.accounts.3c00551.

7. X. Jiang, X. Nie, X. Guo, C. Song, and J. G. Chen, "Recent Advances in Carbon Dioxide Hydrogenation to Methanol via Heterogeneous Catalysis," *Chemical Reviews* 120 (2020): 7984–8034, https://doi.org/10.1021/acs.chemrev.9b00723.

8. R. Ye, J. Ding, T. R. Reina, et al., "Design of catalysts for selective CO_2 hydrogenation," *Nature Synthesis* 4 (2025): 288–302, https://doi.org/10.1038/s44160-025-00747-1.

9. A. Dhakshinamoorthy, S. Navalón, A. Primo, and H. García, "Selective Gas-Phase Hydrogenation of CO_2 to Methanol Catalysed by Metal-Organic Frameworks," *Angewandte Chemie International Edition* 63 (2024): e202311241, https://doi.org/10.1002/anie.202311241.

10. J. Graciani, K. Mudiyanselage, F. Xu, et al., "Highly Active Copper-Ceria and Copper-Ceria-Titania Catalysts for Methanol Synthesis From CO_2," *Science* 345 (2014): 546–550, https://doi.org/10.1126/science.1253057.

11. Y. Liu, D. Deng, and X. Bao, "Catalysis for Selected C1 Chemistry," *Chem* 6 (2020): 2497–2514, https://doi.org/10.1016/j.chempr.2020.08.026.

12. M. Behrens, F. Studt, I. Kasatkin, et al., "The Active Site of Methanol Synthesis Over $Cu/ZnO/Al_2O_3$ Industrial Catalysts," *Science* 336 (2012): 893–897, https://doi.org/10.1126/science.1219831.

13. J. Wang, G. Li, Z. Li, et al., "A highly selective and stable ZnO-ZrO_2 Solid Solution Catalyst for CO_2 Hydrogenation To Methanol," *Science Advances* 3 (2017): e1701290, https://doi.org/10.1126/sciadv.1701290.

14. L.-L. Ling, X. Guan, X. Liu, X.-M. Lei, Z. Lin, and H.-L. Jiang, "Promoted Hydrogenation of CO_2 to Methanol Over Single-Atom Cu Sites With Na^+-Decorated Microenvironment," *National Science Review* 11 (2024): nwae114, https://doi.org/10.1093/nsr/nwae114.

15. B. Xie, R. J. Wong, T. H. Tan, et al., "Synergistic Ultraviolet And Visible Light Photo-Activation Enables Intensified Low-Temperature Methanol Synthesis Over Copper/Zinc Oxide/Alumina," *Nature Communications* 11 (2020): 1615, https://doi.org/10.1038/s41467-020-15445-z.

16. Y. Chai, B. Qin, B. Li, et al., "Zeolite-Encaged Mononuclear Copper Centers Catalyze CO_2 Selective Hydrogenation To Methanol," *National Science Review* 10 (2023): nwad043, https://doi.org/10.1093/nsr/nwad043.

17. S. Kuld, M. Thorhauge, H. Falsig, et al., "Quantifying the Promotion of Cu Catalysts by ZnO for Methanol Synthesis," *Science* 352 (2016): 969–974, https://doi.org/10.1126/science.aaf0718.

18. R. Zhang, X. Wang, K. Wang, et al., "Synthesis of Defect-Rich $La_2O_2CO_3$ Supports for Enhanced CO_2 -to-Methanol Conversion Efficiency," *Science Advances* 10 (2024): eadr3332, https://doi.org/10.1126/sciadv.adr3332.

19. H. Zhou, Z. Chen, A. V. López, et al., "Engineering the Cu/Mo_2CT_x (MXene) Interface to Drive CO_2 Hydrogenation To Methanol," *Nature Catalysis* 4 (2021): 860–871, https://doi.org/10.1038/s41929-021-00684-0.

20. H. Zhao, R. Yu, S. Ma, et al., "The role of Cu_1–O_3 Species in Single-Atom Cu/ZrO_2 Catalyst for CO_2 Hydrogenation," *Nature Catalysis* 5 (2022): 818–831, https://doi.org/10.1038/s41929-022-00840-0.

21. H. Meng, Y. Yang, T. Shen, et al., "Designing Cu^0–Cu^+ dual sites for Improved C–H Bond Fracture Towards Methanol Steam Reforming," *Nature Communications* 14 (2023): 7980, https://doi.org/10.1038/s41467-023-43679-0.

22. H. Li, W. Fang, L.-X. Wang, et al., "Physical Regulation of Copper Catalyst With a Hydrophobic Promoter For Enhancing CO_2 Hydrogenation to Methanol," *The Innovation* 4 (2023): 100445, https://doi.org/10.1016/j.xinn.2023.100445.

23. J. Gong, H. Yue, Y. Zhao, et al., "Synthesis of Ethanol via Syngas on Cu/SiO_2 Catalysts With Balanced Cu^0–Cu^+ Sites," *Journal of the American Chemical Society* 134 (2012): 13922–13925, https://doi.org/10.1021/ja3034153.

24. E. Fernández-Villanueva, P. G. Lustemberg, M. Zhao, J. Soriano Rodriguez, P. Concepción, and M. V. Ganduglia-Pirovano, "Water and Cu^+ Synergy in Selective CO_2 Hydrogenation to Methanol Over Cu–$MgO–Al_2O_3$ Catalysts," *Journal of the American Chemical Society* 146 (2024): 2024–2032, https://doi.org/10.1021/jacs.3c10685.

25. J. Yu, M. Yang, J. Zhang, et al., "Stabilizing Cu^+ in Cu/SiO_2 Catalysts With a Shattuckite-Like Structure Boosts CO_2 Hydrogenation Into Methanol," *ACS Catalysis* 10 (2020): 14694–14706, https://doi.org/10.1021/acscatal.0c04371.

26. J. Zhang, X. Sun, C. Wu, et al., "Engineering $Cu^+/CeZrO_x$ Interfaces to Promote CO_2 Hydrogenation To Methanol," *Journal of Energy Chemistry* 77 (2023): 45–53, https://doi.org/10.1016/j.jechem.2022.10.034.

27. S. Kattel, B. Yan, Y. Yang, J. G. Chen, and P. Liu, "Optimizing Binding Energies of Key Intermediates for CO_2 Hydrogenation to Methanol Over Oxide-Supported Copper," *Journal of the American Chemical Society* 138 (2016): 12440–12450, https://doi.org/10.1021/jacs.6b05791.

28. S. Kattel, P. J. Ramírez, J. G. Chen, J. A. Rodriguez, and P. Liu, "Active sites for CO_2 hydrogenation to methanol on Cu/ZnO catalysts," *Science* 355 (2017): 1296–1299, https://doi.org/10.1126/science.aal3573.

29. Y. Zhou, J. Jiang, Y. Wang, R. Liu, S. Zhang, and J. Wang, "Supercritical CO_2 Activation Enables an Exceptional Methanol Synthesis Activity Over the Industrial $Cu/ZnO/Al_2O_3$ Catalyst," *Advanced Science* 12 (2025): 2500118, https://doi.org/10.1002/advs.202500118.

30. S. Jin, C. Kwon, A. Bugaev, et al., "Atom-by-Atom Design of Cu/ZrO_x Clusters on MgO for CO_2 Hydrogenation Using Liquid-Phase Atomic Layer Deposition," *Nature Catalysis* 7 (2024): 1199–1212, https://doi.org/10.1038/s41929-024-01236-y.

31. I. López-Luque, J. Hack, T. Ródenas, et al., "Engineering Peripheral MetalOxide Catalysis: Interparticle Spacing in Cu/ZrO_2 Catalysts for Methanol Synthesis by CO_2 Hydrogenation," *Angewandte Chemie International Edition* 64 (2025): e202420126, https://doi.org/10.1002/anie.202420126.

32. H. Furukawa, K. E. Cordova, M. O'Keeffe, and O. M. Yaghi, "The Chemistry and Applications of Metal-Organic Frameworks," *Science* 341 (2013): 1230444, https://doi.org/10.1126/science.1230444.

33. H.-C. J. Zhou and S. Kitagawa, "Metal–Organic Frameworks (MOFs)," *Chemical Society Reviews* 43 (2014): 5415–5418, https://doi.org/10.1039/C4CS90059F.

34. X. Zhao, Y. Wang, D.-S. Li, X. Bu, and P. Feng, "Metal–Organic Frameworks for Separation," *Advanced Materials* 30 (2018): 1705189, https://doi.org/10.1002/adma.201705189.

35. L. Jiao and H.-L. Jiang, "Metal-Organic Frameworks for Catalysis: Fundamentals and Future Prospects," *Chinese Journal of Catalysis* 45 (2023): 1–5, https://doi.org/10.1016/S1872-2067(22)64193-7.

36. Q. Yang, Q. Xu, and H.-L. Jiang, "Metal–Organic Frameworks Meet Metal Nanoparticles: Synergistic Effect For Enhanced Catalysis," *Chemical Society Reviews* 46 (2017): 4774–4808, https://doi.org/10.1039/C6CS00724D.

37. L. Li, Z. Li, W. Yang, et al., "Integration of Pd Nanoparticles With Engineered Pore Walls in MOFs for Enhanced Catalysis," *Chem* 7 (2021): 686–698, https://doi.org/10.1016/j.chempr.2020.11.023.

38. G. Li, S. Zhao, Y. Zhang, and Z. Tang, "Metal–Organic Frameworks Encapsulating Active Nanoparticles as Emerging Composites for Catalysis: Recent Progress and Perspectives," *Advanced Materials* 30 (2018): 1800702, https://doi.org/10.1002/adma.201800702.

39. B. An, J. Zhang, K. Cheng, P. Ji, C. Wang, and W. Lin, "Confinement of Ultrasmall Cu/ZnO_x Nanoparticles in Metal–Organic Frameworks for Selective Methanol Synthesis From Catalytic Hydrogenation of CO_2," *Journal of the American Chemical Society* 139 (2017): 3834–3840, https://doi.org/10.1021/jacs.7b00058.

40. S. Hu, J. Huang, M.-L. Gao, et al., "Location-Specific Microenvironment Modulation Around Single-Atom Metal Sites in Metal–Organic Frameworks for Boosting Catalysis," *Angewandte Chemie International Edition* 64 (2025): e202415155, https://doi.org/10.1002/anie.202415155.

41. M. Sun, J. Cheng, A. Anzai, H. Kobayashi, and M. Yamauchi, "Modulating Electronic States of Cu in Metal-Organic Frameworks for Emerging Controllable CH_4/C_2H_4 Selectivity in CO_2 Electroreduction," *Advanced Science* 11 (2024): 2404931, https://doi.org/10.1002/advs.202404931.

42. L.-L. Ling, W. Yang, P. Yan, M. Wang, and H.-L. Jiang, "Light-Assisted CO_2 Hydrogenation Over Pd_3Cu@UiO-66 Promoted by Active Sites in Close Proximity," *Angewandte Chemie International Edition* 61 (2022): e202116396, https://doi.org/10.1002/anie.202116396.

43. G. Yang, W. Shi, Y. Qian, X. Zheng, Z. Meng, and H.-L. Jiang, "Turning on Asymmetric Catalysis of Achiral Metal-Organic Frameworks by Imparting Chiral Microenvironment," *Angewandte Chemie International Edition* 62 (2023): e202308089, https://doi.org/10.1002/anie.202308089.

44. C. Zhang, L. Wang, U. J. Etim, Y. Song, O. M. Gazit, and Z. Zhong, "Oxygen Vacancies in Cu/TiO_2 Boost Strong Metal-Support Interaction and CO_2 Hydrogenation to Methanol," *Journal of Catalysis* 413 (2022): 284–296, https://doi.org/10.1016/j.jcat.2022.06.026.

45. X. Han, T. Xiao, M. Li, et al., "Synergetic Interaction Between Single-Atom Cu and Ga_2O_3 Enhances CO_2 Hydrogenation to Methanol Over $CuGaZrO_x$," *ACS Catalysis* 13 (2023): 13679–13690, https://doi.org/10.1021/acscatal.3c03431.

46. S. Lu, J. Zhang, H. Meng, et al., "Catalytic Direct Dehydrogenation of Ethyl Lactate to Produce Ethyl Pyruvate Over a Synergetic Cu^0/Cu^+ Interface," *Applied Catalysis B: Environmental* 325 (2023): 122329, https://doi.org/10.1016/j.apcatb.2022.122329.

47. X. Liu, X. Wang, S. Zhen, et al., "Support Stabilized PtCu Single-Atom Alloys for Propane Dehydrogenation," *Chemical Science* 13 (2022): 9537–9543, https://doi.org/10.1039/D2SC03723H.

48. D. Gómez, T. Vergara, M. Ortega, et al., "Interdependence Between the Extent of Ga Promotion, the Nature of Active Sites, and the Reaction Mechanism Over Cu Catalysts for CO_2 Hydrogenation to Methanol," *ACS Catalysis* 14 (2024): 15265–15278.

49. J. Li, D. Wang, W. Xiong, J. Ding, and W. Huang, "Interfacial Site Density Engineering of ZnO/Cu Cube Inverse Catalysts for CO_2 Hydrogenation Reactions," *ACS Catalysis* 14 (2024): 17413–17420, https://doi.org/10.1021/acscatal.4c06447.

50. J. Zhang, B. An, Z. Li, et al., "Neighboring Zn–Zr Sites in a Metal–Organic Framework for CO_2 Hydrogenation," *Journal of the American Chemical Society* 143 (2021): 8829–8837, https://doi.org/10.1021/jacs.1c03283.

51. A. Chen, X. Yu, Y. Zhou, et al., "Structure of the Catalytically Active Copper–Ceria Interfacial Perimeter," *Nature Catalysis* 2 (2019): 334–341, https://doi.org/10.1038/s41929-019-0226-6.

52. J. Zhu, Y. Su, J. Chai, V. Muravev, N. Kosinov, and E. J. M. Hensen, "Mechanism and Nature of Active Sites for Methanol Synthesis From CO/CO_2 on Cu/CeO_2," *ACS Catalysis* 10 (2020): 11532–11544, https://doi.org/10.1021/acscatal.0c02909.

53. A. Li, D. Yao, Y. Yang, et al., "Active $Cu^0–Cu^{\sigma+}$ Sites for the Hydrogenation of Carbon–Oxygen Bonds Over Cu/CeO_2 Catalysts," *ACS Catalysis* 12 (2022): 1315–1325, https://doi.org/10.1021/acscatal.1c04504.

54. R. Ye, L. Ma, J. Mao, et al., "A Ce–CuZn Catalyst With Abundant $Cu/Zn–O_V–Ce$ active sites for CO_2 hydrogenation to methanol," *Nature Communications* 15 (2024): 2159, https://doi.org/10.1038/s41467-024-46513-3.

55. V. Dybbert, S. M. Fehr, F. Klein, et al., "Oxidative Fluorination of Cu/ZnO Methanol Catalysts," *Angewandte Chemie International Edition* 58 (2019): 12935–12939, https://doi.org/10.1002/anie.201811267.

56. X. Liu, J. Luo, H. Wang, et al., "In Situ Spectroscopic Characterization and Theoretical Calculations Identify Partially Reduced ZnO_{1-x}/Cu Interfaces for Methanol Synthesis From CO_2," *Angewandte Chemie International Edition* 61 (2022): e202202330, https://doi.org/10.1002/anie.202202330.

57. T. Liu, X. Hong, and G. Liu, "In Situ Generation of the Cu@3D-ZrO_x Framework Catalyst for Selective Methanol Synthesis From CO_2 /H_2," *ACS Catalysis* 10 (2020): 93–102, https://doi.org/10.1021/acscatal.9b03738.

58. Q. Jiang, Y. Liu, T. Dintzer, J. Luo, K. Parkhomenko, and A.-C. Roger, "Tuning the Highly Dispersed Metallic Cu Species via Manipulating Brønsted Acid Sites of Mesoporous Aluminosilicate Support for CO_2 Hydrogenation Reactions," *Applied Catalysis B: Environmental* 269 (2020): 118804, https://doi.org/10.1016/j.apcatb.2020.118804.

59. Y. Yan, R. J. Wong, Z. Ma, et al., "CO_2 hydrogenation to methanol on tungsten-doped Cu/CeO_2 catalysts," *Applied Catalysis B: Environmental* 306 (2022): 121098, https://doi.org/10.1016/j.apcatb.2022.121098.

60. M. Yang, J. Yu, A. Zimina, et al., "Unlocking a Dual-Channel Pathway in CO_2 Hydrogenation to Methanol Over Single-Site Zirconium on Amorphous Silica," *Angewandte Chemie International Edition* 63 (2024): e202312292, https://doi.org/10.1002/anie.202312292.

61. F. C. Meunier, I. Dansette, A. Paredes-Nunez, and Y. Schuurman, "Cu-Bound Formates are Main Reaction Intermediates During CO_2 Hydrogenation to Methanol Over Cu/ZrO_2," *Angewandte Chemie International Edition* 62 (2023): e202303939, https://doi.org/10.1002/anie.202303939.

62. C. Wu, L. Lin, J. Liu, et al., "Inverse ZrO_2/Cu as a Highly Efficient Methanol Synthesis Catalyst From CO_2 Hydrogenation," *Nature Communications* 11 (2020): 5767, https://doi.org/10.1038/s41467-020-19634-8.

Supporting Information

Additional supporting information can be found online in the Supporting Information section.

Supporting File: anie73291-sup-0001-SuppMat.docx.